Random Errors in Turbulence Measurements in the Atmospheric Surface Layer: Implications for Monin–Obukhov Similarity Theory

SCOTT T. SALESKY AND MARCELO CHAMECKI

The Pennsylvania State University, University Park, Pennsylvania

(Manuscript received 19 March 2012, in final form 12 June 2012)

ABSTRACT

An error propagation analysis is conducted to estimate random errors in the friction velocity u_* and the Monin–Obukhov similarity theory (MOST) stability variable z/L from estimated random errors in the turbulent fluxes. Errors in the dimensionless mean wind shear ϕ_m and mean temperature gradient ϕ_h are also estimated. To the authors' knowledge, this is the first time that errors in calculated values of z/L, ϕ_m, and ϕ_h have been systematically analyzed. Random errors in z/L are found to be large for unstable conditions, reaching values of 40% or greater. It is shown through statistical hypothesis tests that random errors cannot explain departures of calculated values of ϕ_m and ϕ_h from theory. The deviation of calculated values of ϕ_m from empirical curves is found to have a strong diurnal variation that increases with height; deviations of ϕ_h from theory are not found to have clear diurnal variation. These results support the findings of previous studies, which have suggested that additional dimensionless parameters representing additional physical processes need to be included in the set of governing parameters for surface layer similarity. Implications for atmospheric surface layer turbulence are also discussed.

1. Introduction

Since the time it was proposed (Obukhov 1946; Monin and Obukhov 1954), the Monin–Obukhov similarity theory (MOST) has been a unifying theory for studies of the atmospheric surface layer (ASL). In MOST, which was developed for the ASL assuming statistically stationary conditions over level, horizontally homogeneous terrain, only four parameters are assumed to be relevant: height z, buoyancy parameter g/Θ_0, kinematic surface stress $-\tau_0/\rho = u_*^2 = (\overline{u'w'}^2 + \overline{v'w'}^2)^{1/2}$, and kinematic surface temperature flux $H_0/\rho c_p = \overline{w'\theta'}$. Application of dimensional analysis reveals that any quantity in the surface layer properly nondimensionalized by these scales should only be a function of the dimensionless MOST stability variable z/L, where

$$L = -\frac{u_*^3 \Theta_0}{\kappa g \overline{w'\theta'}} \tag{1}$$

is the Obukhov length. Here κ is the von Kármán constant. Note that in calculating all quantities, we replace the temperature θ with the virtual temperature θ_v to account for the presence of water vapor, where $\theta_v = \theta(1 + 0.61q)$, and where q is the specific humidity.

MOST provides a framework to interpret experimental results; experiments in the ASL have confirmed that the dimensionless gradients of mean wind ϕ_m and temperature ϕ_h (Businger et al. 1971), and stable spectra of u, v, w, and θ (Kaimal et al. 1972) collapse as a function of z/L. Furthermore, MOST allows one to estimate turbulent fluxes of trace species and water vapor based on mean gradients (e.g., Baldocchi et al. 1988; Moncrieff et al. 1997; Cline 1997) when the eddy covariance technique is not feasible or possible. This gradient-based method is the most reliable approach for obtaining turbulent fluxes of compounds that cannot be measured with high-frequency sensors, such as gaseous mercury (Lee et al. 2000) and volatile organic compounds (Fuentes et al. 2000). MOST is also important for numerical simulations of the atmosphere. It is the basis of parameterized surface fluxes in large-scale numerical models (e.g., Deardorff 1972b; Louis 1979; Beljaars 1995), and for the lower boundary condition in large-eddy simulations (LESs) of the atmospheric boundary layer (e.g., Deardorff 1972a; Moeng 1984). MOST is also the basis for further generalizations, such as the local scaling theory for stable boundary layers (Nieuwstadt 1984).

Corresponding author address: Marcelo Chamecki, Department of Meteorology, The Pennsylvania State University, University Park, PA 16802.
E-mail: chamecki@meteo.psu.edu

DOI: 10.1175/JAS-D-12-096.1

Although scatter in plots of calculated values of ϕ_m and ϕ_h relative to empirical curves is typically assumed to be due to measurement errors, an open question in MOST is to what extent this scatter may be caused by incomplete theory; that is, do ϕ_m and ϕ_h depend on additional dimensionless parameters besides z/L alone? In carefully designed experiments over typical averaging periods (e.g., 30 min) in the surface layer, random errors are expected to be larger than other types of errors (e.g., systematic or instrument errors). Scatter in plots of ϕ_m and ϕ_h is typically assumed to be due to random errors, which are by definition errors that occur due to insufficient averaging time for the time average to converge to the ensemble mean (e.g., Lumley and Panofsky 1964; Wyngaard 1973; Lenschow et al. 1994; Salesky et al. 2012). Estimates of the random errors in ϕ_m and ϕ_h are needed in order to investigate to what extent scatter in plots of ϕ_m and ϕ_h can be explained by random errors. Although some authors have placed error bars on measured MOST functions using bin averaging (e.g., Edson and Fairall 1998), note that this approach does not differentiate between scatter caused by random errors and scatter caused by additional nondimensional parameters representing physical processes that are not accounted for in MOST. Results obtained from LESs (Khanna and Brasseur 1997) and from ABL experiments (Johansson et al. 2001) have demonstrated that ϕ_m depends strongly on and ϕ_h depends weakly on z_i/L under unstable stratification, where z_i is the height of the ABL. However, these results have been questioned by other authors (Andreas and Hicks 2002), who have argued that the relative amount of scatter in plots of ϕ_m and ϕ_h versus z/L is due to spurious correlations between the independent and dependent variables, and therefore it is not possible to demonstrate that z_i/L should enter the scaling. Other authors (Businger 1973; Zilitinkevich et al. 2006) have shown that the roughness length z_0 may become an important length scale as the atmosphere approaches a state of free convection ($u_* \rightarrow 0$), also leading to departures from MOST. In another recent article, Wang and Bras (2010) proposed an extremum solution (ES) to the MOST equations where the momentum flux takes on the value that minimizes the heat flux and wind shear under stable conditions and that minimizes the heat flux and temperature gradient under unstable conditions; they found this solution corresponds to only three possible values that z/L may take on in the surface layer. The conclusions of Wang and Bras (2010) were debated in a comment by van de Wiel et al. (2011) [see also the reply by Wang and Bras (2011)], who argued that a preferred stability state in the stable surface layer is not supported by experimental evidence. If the predictions of Wang and Bras (2010) are correct, then calculated values of z/L that differ from those predicted by the ES must be due to experimental errors in calculated values of z/L.

To investigate the implications of random errors in turbulent fluxes for our understanding of MOST, we perform an error propagation analysis to estimate random errors in the MOST scales u_* and z/L, the mean wind and temperature gradients $\partial U/\partial z$ and $\partial \Theta/\partial z$, and in the dimensionless MOST functions ϕ_m and ϕ_h; expressions for these errors are presented in section 2. The Advection Horizontal Array Turbulence Study (AHATS) dataset and our analysis procedure are discussed in section 3. In section 4, we present the results of the estimated errors in u_*, z/L, $\partial U/\partial z$, $\partial \Theta/\partial z$, ϕ_m, and ϕ_h. Statistical hypothesis tests are conducted to investigate whether scatter in plots of ϕ_m and ϕ_h are due to random error alone; results are presented in section 5. Implications of these random errors for our understanding of the surface layer are given in section 6; a summary of our findings is presented in section 7.

2. Error propagation analysis

In this section, we derive error propagation formulas to estimate random errors in the MOST scales u_* and z/L, in $\partial U/\partial z$ and $\partial \Theta/\partial z$, and in ϕ_m and ϕ_h predicted by MOST. To estimate random errors in turbulent fluxes, we use the filtering method of estimating random error, proposed by Salesky et al. (2012); it has the advantage of not requiring an a priori estimate of the integral time scale as many other methods do. Salesky et al. defined local fluxes using a filter in time of width Δ_t with the property

$$\overline{w'c'} = \overline{\widetilde{w'c'}}; \tag{2}$$

that is, that the time average of the local filtered flux $\widetilde{w'c'}$ is equivalent to the time-averaged flux $\overline{w'c'}$ for any Δ_t. Using this property, they found that the relative random error in $\overline{w'c'}$ for averaging period T can be estimated by

$$\epsilon_{wc} = \frac{C_{wc}}{\overline{w'c'}T^{1/2}}, \tag{3}$$

where C_{wc} is a coefficient determined through a power-law fit of the form $\sigma_{\widetilde{w'c'}}(\Delta_t) = C_{wc}\Delta_t^{-1/2}$ to the standard deviation of the local flux as a function of filter width Δ_t and where the relative error is defined as $\epsilon_{wc} = \sigma_{\overline{w'c'}}/|\overline{w'c'}|$. Note that Salesky et al. (2012) found the random error predicted by the filtering method was similar to other methods (e.g., Lumley and Panofsky 1964; Lenschow et al. 1994; Garcia et al. 2006); consequently, the results given for errors propagated to MOST scales in section 4 are not unique to the filtering method.

Given a variable with a functional dependence on other variables—that is, $c = f(a, b)$ with means $\overline{a}$, $\overline{b}$, and $\overline{c}$, and individual realizations a_i, b_i, and c_i—one can derive an error propagation formula (e.g., Bevington and Robinson 1969) by expanding an individual measurement around its mean in a Taylor series, only retaining linear terms as shown:

$$c_i - \overline{c} \simeq (a_i - \overline{a})\left(\frac{\partial c}{\partial a}\right) + (b_i - \overline{b})\left(\frac{\partial c}{\partial b}\right). \tag{4}$$

By using the definition of variance, $\sigma_c^2 = (1/N)\sum_{i=1}^{N}(c_i - \overline{c})^2$, we can express the variance of c in terms of the variances of a and b and their covariance as

$$\sigma_c^2 \simeq \sigma_a^2\left(\frac{\partial c}{\partial a}\right)^2 + \sigma_b^2\left(\frac{\partial c}{\partial b}\right)^2 + 2\,\mathrm{Cov}(a, b)\frac{\partial c}{\partial a}\frac{\partial c}{\partial b}. \tag{5}$$

The above-mentioned equation is the general error propagation formula that will be used to estimate errors in the following sections.

a. Errors in u_* and z/L

If we apply (5) to estimate the error in the friction velocity, we have $u_* = f(\overline{u'w'}, \overline{v'w'})$ because $u_* = (\overline{u'w'}^2 + \overline{v'w'}^2)^{1/4}$. By (5), the standard deviation of the friction velocity is approximately

$$\sigma_{u_*} \simeq \left[\sigma^2_{\overline{u'w'}}\left(\frac{\partial u_*}{\partial \overline{u'w'}}\right)^2 + \sigma^2_{\overline{v'w'}}\left(\frac{\partial u_*}{\partial \overline{v'w'}}\right)^2 + 2\,\mathrm{Cov}(\overline{u'w'}, \overline{v'w'})\frac{\partial u_*}{\partial \overline{u'w'}}\frac{\partial u_*}{\partial \overline{v'w'}}\right]^{1/2}. \tag{6}$$

In (6), $\mathrm{Cov}(\overline{u'w'}, \overline{v'w'})$ represents the covariance between random errors in $\overline{u'w'}$ and in $\overline{v'w'}$; in principle it could be estimated using the filtering method. However, because it is unclear how one would estimate the error covariance terms in other expressions (e.g., between errors in u_* and $\partial U/\partial z$), we here make the assumption that all errors are uncorrelated and henceforth neglect all the covariance terms that arise from the error propagation equation. Although some of these error covariance terms may be significant, it is unclear to us how one would estimate these terms for each block of data.[1] By taking partial derivatives, and neglecting the covariance term in (6), we find

$$\epsilon_{u_*} = \frac{\sigma_{u_*}}{|u_*|} \simeq \frac{1}{2u_*^4}(\sigma^2_{\overline{u'w'}}\overline{u'w'}^2 + \sigma^2_{\overline{v'w'}}\overline{v'w'}^2)^{1/2} \tag{7}$$

as the expression for the relative random error in u_*. Note that it is typical procedure to rotate velocity data into the mean wind so that $\overline{V} = 0$ at each measurement height. Thus, as Bernardes and Dias (2010) point out, it is valid to assume that the ensemble mean of $\langle v'w' \rangle$ is zero and the sample mean $\overline{v'w'}$ is a random variable with mean zero. One therefore can regard errors in $\overline{u'w'}$ and $\overline{v'w'}$ as uncorrelated. A similar argument does not hold, however, for other error covariance terms.

If we consider z/L, we note that $z/L = f(u_*, \overline{w'\theta'})$. Errors in the mean temperature Θ_0 are small (<0.1% or on the order of 0.3 K; see Salesky et al. 2012) and can be neglected. Applying (5), we find

$$\sigma_{z/L} \simeq \left[\sigma^2_{u_*}\left(\frac{\partial z/L}{\partial u_*}\right)^2 + \sigma^2_{\overline{w'\theta'}}\left(\frac{\partial z/L}{\partial \overline{w'\theta'}}\right)^2\right]^{1/2} \tag{8}$$

as the variance of z/L. Taking derivatives, we find

$$\epsilon_{z/L} = \frac{\sigma_{z/L}}{|z/L|} \simeq \left(\frac{9\sigma^2_{u_*}}{u_*^2} + \frac{\sigma^2_{\overline{w'\theta'}}}{\overline{w'\theta'}^2}\right)^{1/2} \tag{9}$$

as the expression for the relative error in z/L, where σ_{u_*} can be estimated from (7).

b. Errors in gradients

We calculated the gradients of mean wind and temperature by fitting a second-order polynomial in $\ln(z)$ (e.g., Högström 1988) to the measured profiles from the AHATS tower; that is,

$$U(z) = U_0 + A\ln(z) + B[\ln(z)]^2, \tag{10}$$

where U_0, A, and B are determined through least squares. The gradient of mean wind was then obtained by differentiating (10) as shown:

$$\frac{\partial U}{\partial z} = \frac{A}{z} + \frac{2B\ln(z)}{z}. \tag{11}$$

A similar fit to the measured mean temperature profile $\Theta(z)$ was used to obtain $\partial\Theta/\partial z$. One can apply the general error propagation equation (5) to estimate errors in the gradients, noting that for the polynomial fit given in (11), the estimate of the gradient is a function of the fitted parameters A and B; that is, $\partial U/\partial z = f(A, B)$. Applying the error propagation equation (5), we find

[1] One could estimate the error covariance terms in an ensemble mean sense, but this would not allow us to estimate error bars for individual data points.

$$\sigma_{\partial U/\partial z} = \left\{ \sigma_A^2 \left[\frac{\partial(\partial U/\partial z)}{\partial A} \right]^2 + \sigma_B^2 \left[\frac{\partial(\partial U/\partial z)}{\partial B} \right]^2 + 2\,\mathrm{Cov}(A, B) \left[\frac{\partial(\partial U/\partial z)}{\partial A} \right] \left[\frac{\partial(\partial U/\partial z)}{\partial B} \right] \right\}^{1/2}. \quad (12)$$

Taking the derivatives in (12), one can show that the fractional error in the mean wind shear is

$$\epsilon_{\partial U/\partial z} = \frac{\sigma_{\partial U/\partial z}}{|\partial U/\partial z|} = \frac{1}{z|\partial U/\partial z|} \{ \sigma_A^2 + 4[\ln(z)]^2 \sigma_B^2 + 4\,\ln(z)\,\mathrm{Cov}(A, B) \}^{1/2}, \quad (13)$$

where z is height, and σ_A^2, σ_B^2, and $\mathrm{Cov}(A, B)$ are the variances and covariances of the fitted parameters. The method for calculating σ_A^2, σ_B^2, and $\mathrm{Cov}(A, B)$ based on standard statistical methods is given in detail in the appendix. Note that an expression similar to (13) may be used to estimate the error in $\partial\Theta/\partial z$. A simplified form of (13) that only included the σ_A^2 term was used by Johansson et al. (2001) to estimate errors in $\partial U/\partial z$.

c. Errors in ϕ_m and ϕ_h

To determine the implications of random errors for Monin–Obukhov similarity, we here derive formulas for the errors in the dimensionless mean wind shear

$$\phi_m(z/L) = \frac{\kappa z}{u_*} \frac{\partial U}{\partial z} \quad (14)$$

and mean temperature gradient

$$\phi_h(z/L) = \frac{-\kappa z u_*}{\overline{w'\theta'}} \frac{\partial \Theta}{\partial z}. \quad (15)$$

Applying the error propagation equation to $\phi_m = f(u_*, \partial U/\partial z)$, one can show the expression for the relative error in ϕ_m is

$$\epsilon_{\phi_m} = \frac{\sigma_{\phi_m}}{|\phi_m|} \simeq \left[\frac{\sigma_{u_*}^2}{u_*^2} + \frac{\sigma_{\partial U/\partial z}^2}{(\partial U/\partial z)^2} \right]^{1/2} \quad (16)$$

where we have neglected the error covariance term.

An equation for the relative error in ϕ_h can be derived by applying the error propagation formula to $\phi_h = f(u_*, \overline{w'\theta'}, \partial\Theta/\partial z)$. By applying (5), taking derivatives, and neglecting the error covariance terms, one can show that the expression for the relative error in ϕ_h is

$$\epsilon_{\phi_h} = \frac{\sigma_{\phi_h}}{|\phi_h|} \simeq \left[\frac{\sigma_{u_*}^2}{u_*^2} + \frac{\sigma_{\overline{w'\theta'}}^2}{\overline{w'\theta'}^2} + \frac{\sigma_{\partial\Theta/\partial z}^2}{(\partial\Theta/\partial z)^2} \right]^{1/2}. \quad (17)$$

3. Dataset and analysis procedure

ASL data used in this study came from AHATS, collected near Kettleman City, California, during the period from 25 July to 16 August 2008. The terrain surrounding the field site was covered by short grass stubble and was predominantly level and horizontally homogeneous over wind directions of $|\alpha| \leq 45°$ included in the data analysis. The field site was crossed by check dams of 20–25 cm in height and spaced approximately 60 m apart. The closest check dam was approximately 35 m upwind of the AHATS profile tower. We believe the presence of the check dams had no influence on our results, and are confident that the requirements of level and horizontally homogeneous terrain for MOST are satisfied in the AHATS dataset. We used data from the AHATS profile tower, consisting of six Campbell Scientific CSAT-3 triaxial sonic anemometers at heights of z = 1.51, 3.30, 4.24, 5.53, 7.08, and 8.05 m during the period of 25 June–17 July, sampling u, v, w, and θ at 60 Hz. Mean temperature data were collected at 1 Hz at all heights using Sensirion SHT 75 transducers, which were calibrated prior to the field experiment and rechecked after the field campaign. The velocity data for each run were rotated so that $\overline{V} = 0$ for each height. For details of the data selection and processing, see Salesky et al. (2012). The heat flux was calculated using the sonic anemometer data downsampled to 20 Hz; the mean temperature gradient was calculated using the 1-Hz data.

We investigated the possibility of bias in measured values of $\overline{U}$ from the CSAT-3 sonic anemometer data. To determine whether one or more of the anemometers had a bias in mean $\overline{U}$, we assumed that the log law holds for near-neutral ($-0.02 \leq z/L \leq 0.02$) conditions, and compared the average dimensionless mean velocity profile (i.e., $\overline{U}/u_*$) from 22 near-neutral runs to the log law. We found that the fourth and fifth sonic from the profile tower had a positive bias relative to the log law, and assumed that this was due to instrument bias. From fitting a function linear in $\ln(z)$ to the mean dimensionless velocity profile from the remaining heights, we estimated that u had a bias of +0.148 m s^{-1} at z_4 = 5.53 m and a bias of +0.121 m s^{-1} at z_5 = 7.08 m. These biases were removed from the raw data for all runs during preprocessing. We also estimated values of the von Kármán constant and the roughness length from the near-neutral velocity profiles (using the sonics at heights 1–3 and 6 that were free from apparent bias error). We estimated z_0 = 0.0237 m and κ = 0.355 for our data.

Note that although this is on the lower end of reported values of κ in the atmospheric literature, it is comparable with what has been found in some other experiments. Businger et al. (1971) reported a value of $\kappa = 0.35$ for the Kansas data; Oncley et al. (1996) obtained $\kappa = 0.365 \pm 0.015$. We also investigated the possibility of bias in the mean temperature measurements by examining plots of $[\Theta(z) - \Theta_0]/\Theta_0$ and found that the dimensionless mean temperature profiles for near-neutral conditions followed the log law closely. We therefore are confident that the 1-Hz mean temperature data are free from instrument bias.

The filtering method of estimating random errors (Salesky et al. 2012) was applied to the time series of the instantaneous fluxes (e.g., $u'w'$) by downsampling the 60-Hz data to 20 Hz, giving us blocks of 32 768 points, or 27.3 min. We used 50 filter widths spaced evenly on a logarithmic scale, between $\Delta_{\min} = 10\tau_f$, and $\Delta_{\max} = T/10$, where τ_f is the integral time scale of the flux that was estimated by numerically integrating the autocorrelation function $\rho(\tau)$ of the flux up to its first crossing on the time axis.

The gradients of mean wind and temperature were estimated following Högström (1988), where a second-order polynomial in $\ln(z)$ [see (10)] was fit to the measured mean wind profile; this polynomial fit was then differentiated to obtain an approximation to the gradient in (11). We found that for the top five sonics from the AHATS profile, u_* and L did not change with height. When ϕ_m and ϕ_h were calculated, we used the values of u_* and z/L calculated at the height of interest. We used the criteria of Högström (1988), where ϕ_m was only calculated for $u_* > 0.1$ m s^{-1} and ϕ_h was only calculated for runs where $u_* > 0.1$ m s^{-1} and $|H| = |\rho c_p \overline{w'\theta'}| > 10$ W m^{-2}. We found several runs (16 out of 237) with an apparent countergradient heat flux at both heights ($z = 4.24$, 8.05 m) where we calculated $\phi_h(z/L)$; that is, we found $\phi_h(z/L) < 0$ for these cases. The mean temperature profiles and time series of all variables were inspected, and although the cause for these apparent countergradient fluxes is currently unclear, we found they are not due to bad data. We excluded these runs from the χ^2 tests that are presented in section 5 because they would clearly bias the outcome of the χ^2 tests.

4. Results

a. Characterization of ϕ_m and ϕ_h

The behavior of the dimensionless mean wind shear $\phi_m(z/L)$ is displayed in Fig. 1, with all stabilities shown in Fig. 1a and the near-neutral cases presented in Fig. 1b. Each data point is plotted for $\phi_m(z/L)$ calculated from one 27.3-min block of data. The empirical functions

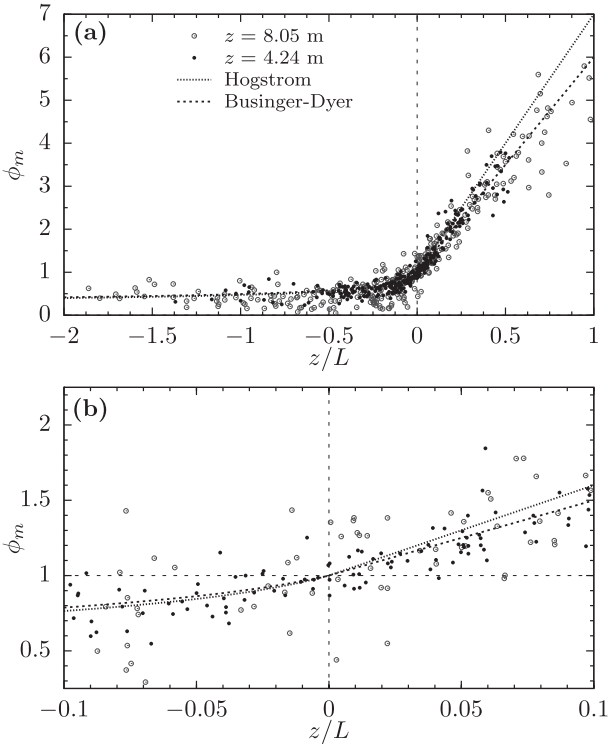

FIG. 1. Dimensionless mean wind shear as a function of MOST stability variable: (a) $-2 \le z/L \le 1$ and (b) $-0.1 \le z/L \le 0.1$.

proposed by Businger and Dyer (Dyer 1974) and Högström (1988) are also shown for comparison. Although the scatter in ϕ_m is larger than what has been found in some experiments (e.g., Businger et al. 1971; Högström 1974, 1988), it is similar to what has been found in many other ASL studies, such as the results of Johansson et al. (2001) and Li et al. (2008). Notice that the scatter in ϕ_m increases with height; it is larger for measurements at $z = 8.05$ m than for $z = 4.24$ m. Also note that calculated values of ϕ_m plotted in Fig. 1 are plotted using $\kappa = 0.355$, which was fit from the near-neutral velocity profiles.

The dimensionless mean temperature gradient is displayed in Fig. 2, with stabilities from $-2 \le z/L \le 1$ displayed in Fig. 2a and near-neutral ($-0.1 \le z/L \le 0.1$) data shown in Fig. 2b. The empirical Businger–Dyer (Dyer 1974) and Högström (1988) curves are also displayed for comparison. We find much less scatter in calculated values of ϕ_h for unstable conditions than for ϕ_m, and by inspection of Fig. 2a, one would likely conclude that the data are in very good agreement with both sets of empirical curves for unstable conditions. For stable conditions, there is much more scatter in ϕ_h, and there is also a negative bias in calculated values of ϕ_h relative to both the Högström and Businger–Dyer curves. Note that for near-neutral conditions, displayed

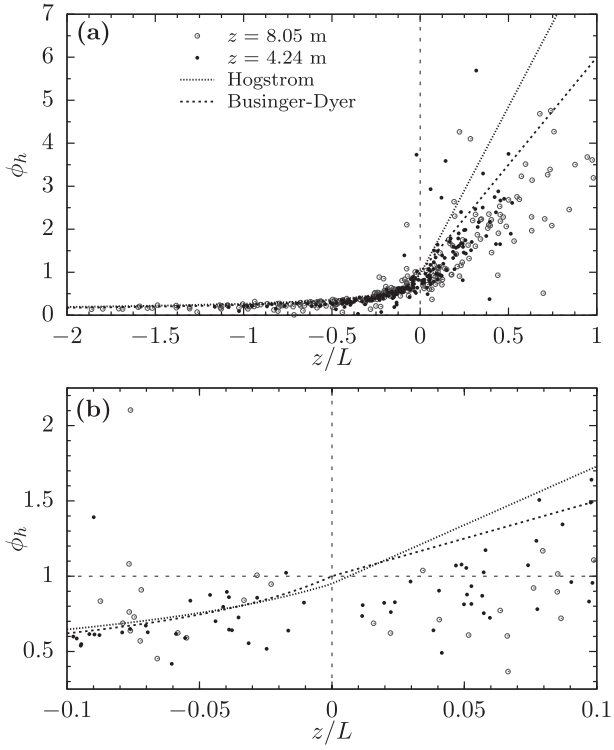

FIG. 2. Dimensionless mean temperature gradient as a function of MOST stability variable: (a) $-2 \le z/L \le 1$ and (b) $-0.1 \le z/L \le 0.1$.

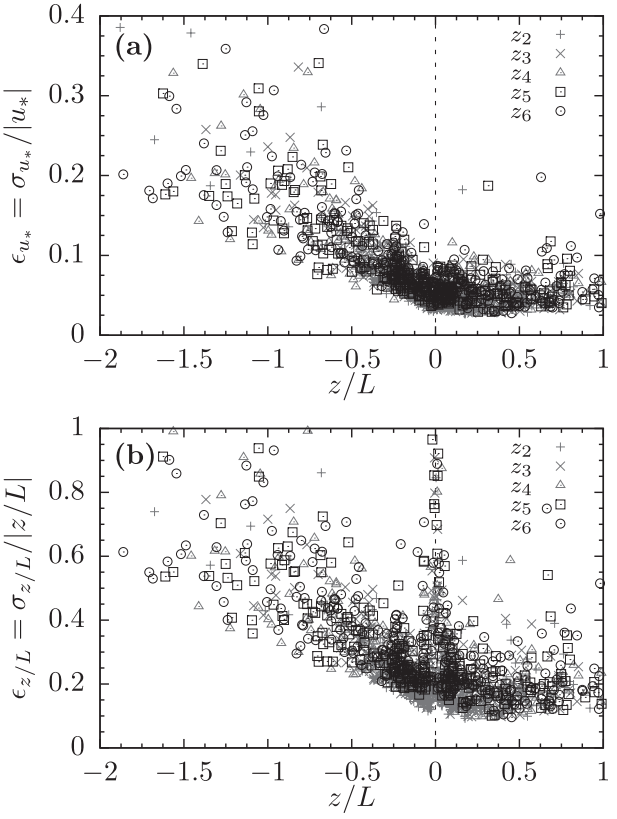

FIG. 3. Relative random error in (a) the friction velocity and (b) the MOST stability variable from the filtering method for the top five heights from the AHATS profile tower as a function of z/L.

in Fig. 2b, most calculated values of ϕ_h are less than one and smaller than the empirical predictions. Our results in Figs. 1, 2 therefore suggest that a turbulent Prandtl number ($\mathrm{Pr}_t = \phi_h/\phi_m$) of less than one is appropriate for near-neutral conditions in the atmospheric surface layer.

b. Errors in z/L and u_*

The errors in $\overline{u'w'}$, $\overline{v'w'}$, and $\overline{w'\theta'}$ were calculated using the filtering method at the top five levels from the AHATS profile tower and propagated to u_* and z/L using (7) and (9). The relative error in u_* is plotted in Fig. 3a as a function of z/L; the relative error in z/L is shown in Fig. 3b. Neither errors in u_* or in z/L were found to have an apparent height dependence. In Fig. 3a, errors in u_* are approximately constant and small for stable conditions, with typical values around 3%–5%. Errors in u_* increase with increasing atmospheric instability; they may become as large as 10%–20% for unstable conditions. The errors in u_* are primarily due to random errors in $\overline{u'w'}$; we found the second term in (7) was typically less than 10% the magnitude of the first term. Note also that the error in u_* increases with increasing instability both because $u_* \to 0$ in the free convective limit and because $\sigma_{\overline{u'w'}}$ increases with increasing instability.

Errors in z/L, shown in Fig. 3b, are smallest for stable stratification, with values ranging from 10% to 20%. However, errors in z/L can become large with increasing instability, reaching values of 50% or greater. Note that the relative error in z/L is proportional to $1/u_*^3$ and therefore increases rapidly with increasingly negative values of z/L, since $u_* \to 0$ in the free convective limit. The errors in both u_* and z/L exhibit more scatter for the unstable cases in Fig. 3. This is due to the large errors in z/L for unstable conditions, which prevent a more clear collapse of the data points when plotted against z/L.

c. Errors in gradients

Errors in $\partial U/\partial z$ were estimated based on (13); errors in $\partial\Theta/\partial z$ were estimated based on a similar expression. The estimated errors in the gradients are displayed in Fig. 4a for $\partial U/\partial z$ and in Fig. 4b for $\partial\Theta/\partial z$. Errors in the mean velocity gradient, given in Fig. 4a, are typically on the order of 20% or less for stable stratification. For unstable stratification, however, errors in $\partial U/\partial z$ are highly variable for any given stability; errors here can be negligible or as large as 50% or greater. The large errors

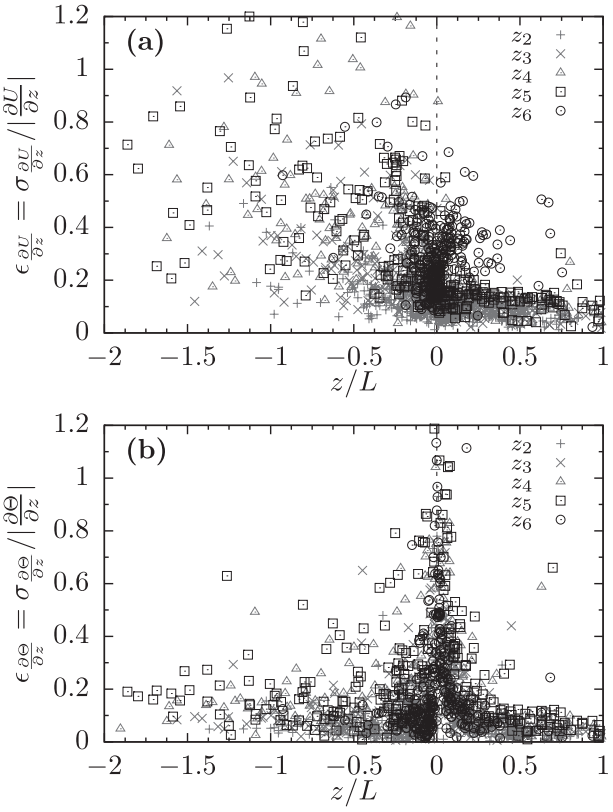

FIG. 4. Relative random error in (a) the gradient of mean wind and (b) the mean temperature gradient.

in $\partial U/\partial z$ that can be seen in Fig. 4a occur when the polynomial fit in $\ln(z)$ to the measured mean velocity profile is poor. However, these large errors are likely an overestimate of the true random error, since the true $\partial U/\partial z$ is not necessarily a second-order polynomial in $\ln(z)$, even in the absence of any random error. Errors in the mean temperature gradient, displayed in Fig. 4b, are typically on the order of 15% or less for stable conditions and 30% or less for unstable conditions. For near-neutral stratification, relative errors in $\partial\Theta/\partial z$ become large because $|\partial\Theta/\partial z| \to 0$ as $z/L \to 0$.

d. Errors in ϕ_m and ϕ_h

Errors in $\phi_m(z/L)$ predicted by MOST are displayed in Fig. 5. Each data point represents the value of $\phi_m(z/L)$ calculated for one 27.3-min block of data; error bars, plotted for one standard deviation, are calculated from (16) for ϕ_m and from (9) for z/L. The empirical functions of Businger and Dyer (Dyer 1974) and Högström (1988) are also displayed for comparison. In Figs. 5a,b, $\phi_m(z/L)$ is plotted for measurements calculated at a height of $z = 4.24$ m; Figs. 5c,d are for measurements at $z = 8.05$ m. Note that z/L is plotted on a logarithmic scale. For many of the unstable points in Fig. 5a,c, the vertical error bars on $\phi_m(z/L)$ are outside of both sets of empirical curves. Although the horizontal error bars are also large for the unstable cases, the empirical functions vary slowly with z/L, so even these large random errors in z/L do not appear to be large enough to explain the departures in calculated values of $\phi_m(z/L)$ from the empirical functions. Stable cases, displayed in Figs. 5b,d, have a similar behavior; the empirical curves are not contained within the error bars for many of the data points. From Fig. 5, we make the qualitative observation that random errors in both ϕ_m and z/L do not appear to be able to explain the scatter in $\phi_m(z/L)$ relative to the empirical functions; it suggests that mechanisms in addition to random error are responsible for the scatter observed in $\phi_m(z/L)$. The differences between calculated values of $\phi_m(z/L)$ and the empirical functions will be analyzed quantitatively through a χ^2 test in section 5b.

A plot of $\phi_h(z/L)$ is displayed in Fig. 6. Once again, Figs. 6a,b are for measurements taken at $z = 4.24$ m and Figs. 6c,d for measurements at $z = 8.05$ m. Error bars for z/L are plotted based on (9); error bars for ϕ_h are plotted using (17). The empirical Businger–Dyer and Högström curves are also displayed in Fig. 6. Note that in general, calculated values of $\phi_h(z/L)$ have a negative bias relative to both sets of empirical curves displayed in Fig. 6. Much less scatter is found for unstable ϕ_h (Figs. 6a,c) relative to the empirical functions than what was observed for ϕ_m, but the vertical error bars are also smaller. For the stable cases (Figs. 6b,d), ϕ_h once again has a negative bias, which is not in as good agreement with either the Businger–Dyer or the Högström functions as for the unstable cases. However, calculated values of ϕ_h do vary systematically with z/L for stable cases, even though they are not in agreement with the existing empirical functions we considered here.

5. Implications for MOST

a. MO extremum solution

One of the implications of the extremum solution of Wang and Bras (2010) is that the MOST stability parameter must take on one of the discrete values $z/L^{\mathrm{ES}} = -0.2, 0.0, 0.1$. The conclusions of Wang and Bras (2010) were disputed by van de Wiel et al. (2011), who argued that experimental results do not support a favored stability state in the stable surface layer. In reply to the comments of van de Wiel et al. (2011), Wang and Bras (2011) presented a bimodal frequency distribution of z/L with peaks for one stable and one unstable value of z/L. If the extremum hypothesis of Wang and Bras (2010) is correct, then any observed deviations from $z/L = z/L^{\mathrm{ES}}$ must be due to measurement error (either systematic or random) when z/L is calculated from data for conditions

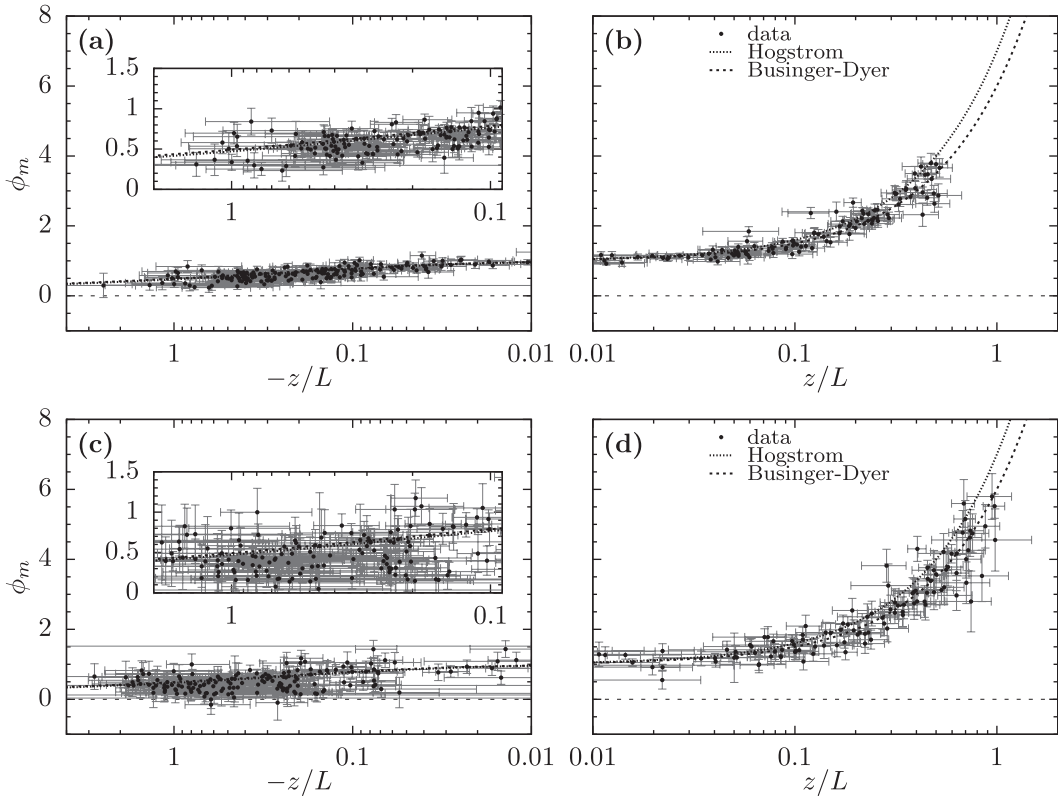

FIG. 5. The dimensionless velocity gradient shown as a function of the MO stability variable with error bars for both terms: (a) $z = 4.24$ m, unstable; (b) $z = 4.24$ m, stable; (c) $z = 8.05$ m, unstable; and (d) $z = 8.05$ m, stable.

under which MOST holds. The error propagation analysis presented in section 2 allows us to estimate $\sigma_{z/L}$ and therefore test the prediction of the extremum solution that z/L must take on one of the discrete values $z/L^{\mathrm{ES}} = -0.2, 0.0, 0.1$.

We test this prediction of the ES by performing a χ^2 test of the null hypothesis that $z/L = z/L^{\mathrm{ES}}$. Here the test statistic

$$X^2 = \sum_N \left(\frac{z/L^{\mathrm{ES}} - z/L}{\sigma_{z/L}} \right)^2 \tag{18}$$

is compared to a χ^2 distribution with N degrees of freedom, where z/L^{ES} is the value of z/L given by the extremum solution and z/L and $\sigma_{z/L}$ are the measured value and standard deviation of z/L from the AHATS data, respectively. Here the calculated value of z/L was compared to the closest value of $z/L^{\mathrm{ES}} = -0.2, 0.0, 0.1$. We obtain the value of $X^2(N = 277) = 1975.4$, $(p < 0.01)$ for the test statistic, where p is the probability of falsely rejecting the null hypothesis. Hence, the χ^2 test indicates that we can reject the null hypothesis at a high (99.9%) confidence level in favor of the alternative, namely, that the values of z/L predicted by the extremum solution of Wang and Bras (2010) are not in agreement with observed values from the AHATS dataset.

b. *Do ϕ_m and ϕ_h depend on z/L alone?*

According to the classical formulation of MOST, quantities in the surface layer suitably nondimensionalized by the relevant scales should be quantities of the dimensionless stability parameter z/L alone. However, it is well known (Kaimal et al. 1972) that the spectra of u and v in the unstable regime do not collapse as a function of z/L; their variances therefore also fail to follow MOST. Panofsky et al. (1977) and Banta (1985) provided evidence that the horizontal velocity variances σ_u^2 and σ_v^2 have a dependence on z_i/L. Khanna and Brasseur (1997) investigated the departure of other surface layer quantities from MOST scaling in the unstable surface layer using LES. They found that $\phi_m \sim O(1)$ for the values of z_i/L that they considered, which indicated that MOST scales were appropriate for nondimensionalization; however, systematic variation was observed for the various z_i/L values, suggesting that $\phi_m = f(z/L, z_i/L)$. The dimensionless temperature gradient ϕ_h was found to be in good agreement with MOST, collapsing neatly for different z_i/L values. Johansson

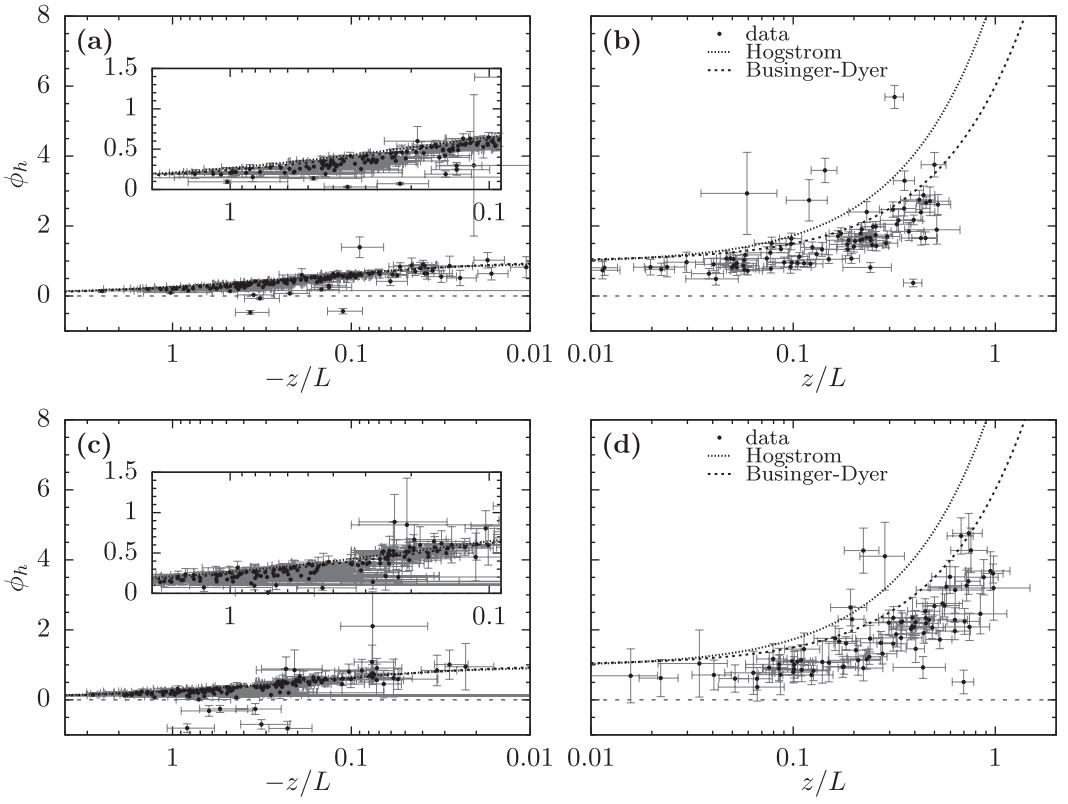

FIG. 6. The dimensionless temperature gradient shown as a function of the MO stability variable with error bars for both terms: (a) $z = 4.24$ m, unstable; (b) $z = 4.24$ m, stable; (c) $z = 8.05$ m, unstable; and (d) $z = 8.05$ m, stable.

et al. (2001) examined departures from MOST for ϕ_m and ϕ_h using ASL data together with estimates of z_i obtained from aircraft data. They also found a systematic variation in ϕ_m with z_i/L in addition to the expected z/L dependence. In contrast to Khanna and Brasseur (1997), they found that ϕ_h did have an evident dependence on z_i/L, although it was weaker than what was observed for ϕ_m. Andreas and Hicks (2002) argued that this difference between the scatter in ϕ_m and ϕ_h relative to the empirical curves is due to spurious correlations, since u_* appears in both the independent and dependent variable in plots of ϕ_m or ϕ_h against z/L. They assumed a 10% error in u_* and showed that it would move a point away from the $z/L - \phi_m$ curve but along the $z/L - \phi_h$ curve, and concluded that the difference in scatter that Johansson et al. (2001) found between ϕ_m and ϕ_h could not be clearly attributed to z_i/L dependence. In their reply, Johansson et al. (2002) pointed out that Andreas and Hicks (2002) neglected the possibility of random errors in $\overline{w'\theta'}$ and showed that the combination of errors in u_* and $\overline{w'\theta'}$ could have a complex influence on a point in the $z/L - \phi_m$ or $z/L - \phi_h$ plane. However, they assumed values of errors in u_* and $\overline{w'\theta'}$ instead of estimating them directly from the data.

The error propagation analysis presented above allows us to quantify random errors in both the independent and dependent variables in plots of ϕ_m and ϕ_h as a function of z/L. We therefore are able to directly test whether the observed scatter in calculated values of ϕ_m and ϕ_h relative to the empirical functions can be explained solely by random error. We perform a χ^2 test of the null hypothesis that calculated values of the MOST ϕ functions from AHATS that are in agreement with the empirical Businger–Dyer curves (Dyer 1974). We perform the test with regard to variability in z/L and ϕ_m or ϕ_h separately; that is, for ϕ_m we first test the hypothesis using the test statistic

$$X^2_{\phi_m} = \sum_N \left(\frac{\phi_m^{\text{emp}} - \phi_m^{\text{meas}}}{\sigma_{\phi_m}} \right)^2, \tag{19}$$

where ϕ_m^{emp} is the value of $\phi_m(z/L)$ from the empirical function, ϕ_m^{meas} is the measured value from the AHATS data, and σ_{ϕ_m} is the standard deviation of ϕ_m calculated from the AHATS data, estimated using (16). We then test the hypothesis with regard to variability in z/L, that is, using the test statistic

TABLE 1. Results from χ^2 test of agreement between $\phi_m(z/L)$ and the empirical Businger–Dyer function (Dyer 1974). P3 denotes measurements at $z = 4.24$ m from the profile, P6 denotes measurements at $z = 8.05$ m, N is the number of degrees of freedom, $X^2_{\phi_m}$ is the test statistic using variability in ϕ_m, $X^2_{z/L}$ is the test statistic using variability in z/L, and p_{ϕ_m} and $p_{z/L}$ are the p values for each of the two tests respectively, i.e., the probability of falsely rejecting the null hypothesis.

Sonic	N	$X^2_{\phi_m}$	p_{ϕ_m}	$X^2_{z/L}$	$p_{z/L}$
P3, unstable	161	374.3	<0.01	3.30×10^4	<0.01
P3, stable	115	255.4	<0.01	1.36×10^3	<0.01
P6, unstable	157	296.9	<0.01	7.69×10^{16}	<0.01
P6, stable	116	161.8	<0.01	1.01×10^5	<0.01

TABLE 2. Results from χ^2 test of agreement between $\phi_h(z/L)$ and the empirical Businger–Dyer function (Dyer 1974). P3 denotes measurements at $z = 4.24$ m from the profile, P6 denotes measurements at $z = 8.05$ m, N is the number of degrees of freedom, $X^2_{\phi_h}$ is the test statistic using variability in ϕ_h, $X^2_{z/L}$ is the test statistic using variability in z/L, and p_{ϕ_h} and $p_{z/L}$ are the p values for each of the two tests respectively, i.e., the probability of falsely rejecting the null hypothesis.

Sonic	N	$X^2_{\phi_h}$	p_{ϕ_h}	$X^2_{z/L}$	$p_{z/L}$
P3, unstable	136	2517	<0.01	6.58×10^5	<0.01
P3, stable	82	703.2	<0.01	5.23×10^3	<0.01
P6, unstable	132	402.7	<0.01	7.55×10^6	<0.01
P6, stable	80	279.4	<0.01	2.95×10^3	<0.01

$$X^2_{z/L} = \sum_N \left(\frac{z/L^{\text{emp}} - z/L^{\text{meas}}}{\sigma_{z/L}} \right)^2, \qquad (20)$$

where z/L^{emp} is the empirical value of z/L from the Businger–Dyer function for a given value of ϕ_m, z/L^{meas} is the value of z/L from the AHATS data, and $\sigma_{z/L}$ is its standard deviation estimated from (9). We perform these two hypothesis tests separating the two heights from the AHATS profile tower for which we plot $\phi_m(z/L)$ in Fig. 5 and considering stable and unstable cases separately. We limited the stabilities considered to $-2 \le z/L \le 1$, since this is the typical range over which the empirical MOST functions are defined (e.g., Foken 2006).

Results of the χ^2 hypothesis test comparing calculated values of ϕ_m to the empirical Businger–Dyer function (Dyer 1974) are displayed in Table 1. For stable and unstable stratification at both heights, we obtain p values of $p < 0.01$ both when the χ^2 test is conducted with regard to variability in ϕ_m and with regard to variability in z/L. From the results given in Table 1, we are able to reject the null hypothesis at a high level (99%) of confidence in favor of the alternative, that is, that $\phi_m(z/L)$ does not agree with the empirical Businger–Dyer function. Note that the scatter in Fig. 5 (in particular, Figs. 5a,b) and in Fig. 1 are typical of ASL experimental data. Visual inspection of Fig. 5 without error bars or Fig. 1 alone would likely lead one to the conclusion that both empirical curves displayed in the figures are a good fit to the data. The χ^2 hypothesis tests were also conducted using the empirical curve of Högström (1988), and an empirical curve that was fit to the AHATS dataset. In both cases, although the values of the test statistics were slightly different, the p values remained unchanged, which give us confidence that our conclusions are robust.

These χ^2 tests indicate that random errors are not able to fully account for the variability in $\phi_m(z/L)$ either for unstable or stable conditions and suggest that ϕ_m may also be a function of some dimensionless parameter that describes physical processes that are neglected in MOST, in addition to z/L. Potential candidates for this additional parameter in the convective boundary layer include z/z_0 and z/z_i. The variability in ϕ_m for stable conditions also cannot be fully explained by random error. This once again may indicate that ϕ_m depends on dimensionless parameters besides z/L alone, or that other processes in the stable boundary layer contribute to departures from MOST (e.g., Cheng et al. 2005).

Calculated values of the test statistics for the χ^2 test for ϕ_h are displayed in Table 2. Here we find very small (<0.01) p values for the test with regard to variability in z/L for all cases tested. When the test was conducted with regard to variability in ϕ_h, we again found small (<0.01) p values for unstable and stable cases at both heights. Note that the outliers evident in Fig. 6 that would clearly skew the results (e.g., points where $z/L < 0.2$ and $\phi_h > 2.5$ in Fig. 6b) were excluded from the χ^2 test. Because the data points in Fig. 6 have a negative bias relative to the empirical curves of both Högström (1988) and Businger–Dyer (Dyer 1974), we also performed the χ^2 tests using an empirical curve that is the best fit to measured values of ϕ_h from AHATS. However, although the values of the test statistics were slightly different in this case, we still obtain small (<0.01) p values for all of the χ^2 tests.

For ϕ_h, as with ϕ_m, the results of the χ^2 tests indicate that random error does not fully explain the amount of scatter in plots of $\phi_h(z/L)$, even though there is much less scatter in unstable ϕ_h than for ϕ_m. These results suggest that it may be possible to find additional nondimensional parameters describing additional physical processes that should be accounted for in ϕ_h.

c. Possible cause of deviations from MOST

From the error analysis presented above, and the χ^2 tests that were used to quantify agreement between calculated values of the dimensionless gradients and the

empirical functions, it is evident that random errors are not able to explain the deviations from MOST that are observed. Because the observed scatter in ϕ_m and ϕ_h cannot be explained by random errors, these deviations from MOST must be due to either the violation of assumptions required for MOST (i.e., a level surface, stationarity, horizontal homogeneity) or the dependence of ϕ_m and ϕ_h on additional dimensionless parameters besides z/L that are related to the physical processes that lead to these deviations from MOST.

Because we excluded nonstationary periods from our analysis [using the criteria of Vickers and Mahrt (1997)], it is unlikely that we are violating the stationarity assumption. Based on the level topography and short vegetation present at the AHATS field site, it is also unlikely that a sloping surface or horizontal inhomogeneities contributed to the observed deviations of calculated values of unstable ϕ_m from MOST. We plotted the normalized deviation of ϕ_m from the empirical function [e.g., $(\phi_m^{\text{emp}} - \phi_m^{\text{meas}})/\phi_m^{\text{emp}}$, where ϕ_m^{emp} is the empirical form and ϕ_m^{meas} is the calculated value from AHATS] against wind angle. We found that the normalized deviation of ϕ_m from MOST did not have any evident dependence on wind angle, so the requirements of horizontal homogeneity and a level surface do indeed appear to be satisfied. The same was found to hold true for ϕ_h.

The observed deviations of ϕ_m and ϕ_h from MOST therefore appear to be due to physical processes that are not accounted for in MOST. We find that the deviations of ϕ_m from MOST have diurnal variation. Results from AHATS are displayed in Fig. 7, where in Figs. 7a,b the normalized deviation of ϕ_m from MOST [i.e., $(\phi_m^{\text{emp}} - \phi_m^{\text{meas}})/\phi_m^{\text{emp}}$, where the Businger–Dyer empirical curve is used] is plotted as a function of local time [Pacific daylight time (PDT)] with different symbols used for the stable and unstable points. The black points showing the diurnal trend are calculated from 90-min bin averages, where the error bars indicate the standard deviation within each bin. Average times of sunrise and sunset during the course of the AHATS experiment are shown with vertical lines. We observe that the normalized deviation of ϕ_m from MOST for the stable points is distributed around zero. However, the deviation from MOST varies systematically with time of day for the unstable points. In general, the deviation of calculated values of ϕ_m from MOST is negative ($\phi_m^{\text{emp}} < \phi_m^{\text{meas}}$) in the first several hours in the morning after sunrise; it becomes positive ($\phi_m^{\text{emp}} > \phi_m^{\text{meas}}$) in the early afternoon and then decreases to around zero before sunset. The deviations from MOST are larger at $z = 8.05$ m (Fig. 7b) than for $z = 4.24$ m (Fig. 7a). The deviations of calculated values from the empirical functions for measurements at $z = 8.05$ m may be as large as 50% during the daytime for the bin-averaged values (deviations for individual data points may be 100% or greater). Although the error bars for the bin-averaged values may be large for some of the unstable points, a clear diurnal trend is still evident, especially for $z = 8.05$ m as displayed in Fig. 7b.

In Fig. 7c, the bin-averaged deviations of ϕ_m from empirical curves are plotted for the top five heights from the AHATS profile tower. The bin-averaged deviations of calculated values of ϕ_m are found to vary diurnally, and these deviations increase systematically with height. In Fig. 7d, a similar plot is presented for the bin-averaged deviations of ϕ_h from the empirical curves. Here the deviations of ϕ_h from MOST show no clear diurnal variation as with ϕ_m and very little dependence on measurement height. Recall that in Figs. 2, 6, the calculated values of ϕ_h had a systematic negative bias relative to the empirical curves; this fact is also evident in Fig. 7d. The lack of clear diurnal variation in the deviations of ϕ_h from MOST suggest that, although random error cannot fully explain the deviations of ϕ_h from theory, ϕ_h does not appear to depend on some dimensionless quantity that varies diurnally. However, ϕ_h does have a clear positive deviation near sunset, which suggests that processes related to the collapse of the convective boundary layer may lead to large deviations of ϕ_h from theory.

From Fig. 7, it is evident that the deviations of ϕ_m from MOST under unstable stratification depend systematically on some quantity that varies diurnally. Potential candidates for this additional parameter include water vapor mixing ratio, mean temperature, the surface heat flux, the presence of clouds, and the boundary layer depth. Another possible candidate is z_0, which may become an important length scale under free convective conditions ($u_* \to 0$). However, because the deviations of ϕ_m from MOST increase with height as shown in Fig. 7c, we believe it is unlikely that the deviations in ϕ_m from theory that we observe depend on z/z_0. While one plausible candidate that is consistent with previous studies (Khanna and Brasseur 1997; Johansson et al. 2001) is z_i, we cannot conclusively determine what the missing scale is from our present data; we hope to investigate it in a future study.

6. Discussion

The large random errors that are found for unstable z/L (displayed in Fig. 3a) are significant for any study where MOST scaling is used and the dependent dimensionless variable is plotted as a function of z/L. For example, one can see that for $z/L = -1$, the relative random error (defined as $\epsilon_{z/L} = \sigma_{z/L}/|z/L|$) in z/L is 40%; thus, if one

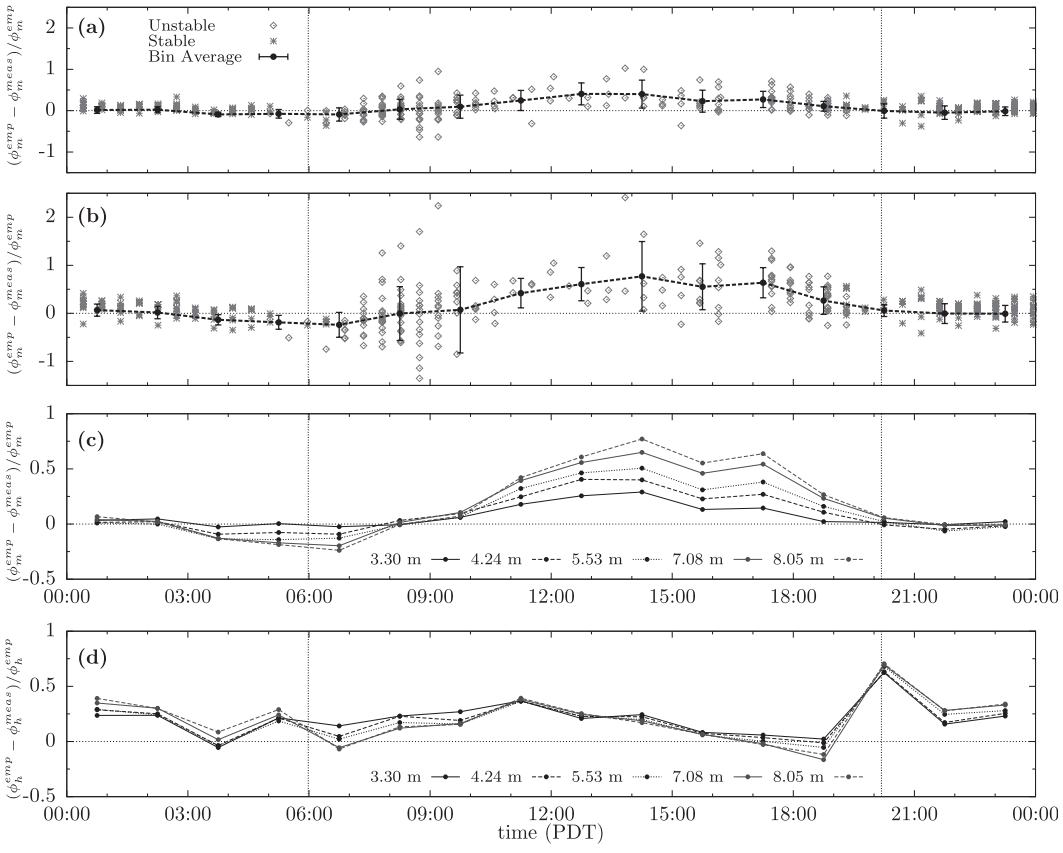

FIG. 7. Diurnal variation of normalized deviations of ϕ_m and ϕ_h from the empirical Businger–Dyer functions (Dyer 1974). (a),(b) Gray points indicate the normalized deviation from the empirical ϕ_m function for each 27.3-min block of data; black points are the bin-averaged deviations. Vertical dashed lines indicate the average times of sunrise and sunset during the course of the AHATS experiment. (a) ϕ_m, $z = 4.24$ m; (b) ϕ_m, $z = 8.05$ m. (c) Bin-averaged ϕ_m for top five sonics from AHATS profile tower. (d) Bin-averaged ϕ_h. Note that the scale on the ordinate is different for (c),(d) than for (a),(b).

calculates $z/L = -1$ based on time-averaged fluxes, there is a 68% probability that the true ensemble mean value of z/L lies between $z/L = -1.4$ and -0.6. Thus, for unstable stratification, the true value of z/L is difficult to determine accurately for typical averaging periods in the ASL (recall we are calculating time averages over blocks of $T = 27.3$ min in length). However, note that for unstable stratification, the random errors in z/L do not affect agreement with the empirical functions greatly for ϕ_m and ϕ_h, because the empirical functions vary slowly with z/L for unstable stratification (see Figs. 5a,c, 6a,c). Random errors in z/L are less of an issue for stable stratification, where they are typically on the order of 10%.

These large random errors found in z/L for unstable conditions may also explain in part why the empirical curves for the spectra of u, v, w, and θ proposed by Kaimal et al. (1972) fail to collapse for unstable conditions. For example, the nondimensional w spectrum collapses as a function of z/L for $-0.3 \leq z/L \leq 2.0$, but for $z/L < -0.3$ the w spectrum does not collapse but rather is ordered randomly within a shaded region for any given period of data. It is possible that the w spectrum does have systematic behavior with z/L for unstable conditions, but this fact is obscured by the random errors in z/L, which make the true ensemble mean value of z/L difficult to determine accurately. This also could be the cause of the shaded region in the w spectrum. However, the spectra may also fail to collapse due to other factors, such as the presence of mesoscale motions, or the potential influence of z_i. Random errors in z/L may also contribute to the shaded regions in the u and v spectra, although this conclusion should be viewed with some caution because it is known that σ_u^2 and σ_v^2 (and therefore the u and v spectra) scale with z_i (Panofsky et al. 1977; Banta 1985). The shaded regions for the u and v spectra therefore may be due to a combination of random errors in z/L, scaling with z_i, and other factors.

Our results suggest that the true value of ϕ_m (based on time averages) is a function of both z/L and some additional parameter α, for example, $\phi_m^{\text{true}} = \phi_m^{\text{true}}(z/L, \alpha)$. The relationship between this true value of ϕ_m and the calculated value of ϕ_m from experimental data is

$$\phi_m^{\text{calc}}(z/L) = \int \phi_m^{\text{true}}(z/L, \alpha) P(\alpha)\, d\alpha, \qquad (21)$$

where $P(\alpha)$ is the probability density function of the parameter α for a given dataset. Thus, if one has a biased sample of α, then this could lead to a bias in the calculated value of $\phi_m(z/L)$. This could explain the differences between empirical curves that have been fit to calculated values of $\phi_m(z/L)$ from different datasets. This may also explain why the scatter in ϕ_m and ϕ_h from the Kansas experiment (Businger et al. 1971) and from Högström (1974) was found to be smaller than in many other studies. For both the Kansas experiment and Högström (1974), data collection was limited to summer afternoon periods due to logistical constraints (Johansson et al. 2002).

A number of articles (e.g., Andreas and Hicks 2002; Klipp and Mahrt 2004; Baas et al. 2006) have discussed the role of self-correlation in the relative amounts of scatter in plots of $\phi_m(z/L)$ and $\phi_h(z/L)$. Self-correlation occurs when there is error in a common variable that is used to normalize both the independent and dependent variable, that is, u_* in plots of $\phi_m(z/L)$ or $\phi_h(z/L)$ and $\overline{w'\theta'}$ in plots of $\phi_h(z/L)$. Andreas and Hicks (2002) showed that for unstable stratification, an error in u_* would move a point in the $\phi_m - z/L$ plane along empirical curves (because $\phi_m \propto 1/u_*$), and would move a point in the $\phi_h - z/L$ plane away from empirical curves (because $\phi_h \propto u_*$). Baas et al. (2006) examined the more general case of combinations of errors in u_* and $\overline{w'\theta'}$, and concluded that, in general, errors in u_* and $\overline{w'\theta'}$ would lead to inherently more scatter in unstable ϕ_m and stable ϕ_h and less scatter in unstable ϕ_h and stable ϕ_m.

The results of Baas et al. (2006) have several implications for the present article. First, because self-correlation decreases the scatter in unstable ϕ_h and stable ϕ_m, and because these cases still do not pass our χ^2 tests, we believe that our conclusions for unstable ϕ_h and stable ϕ_m are robust. If the effects of self-correlation were removed, then the observed scatter would increase, and these cases still would not pass the χ^2 tests. For unstable ϕ_m, it is possible that self-correlation is one factor leading to the large amount of scatter that is observed. However, we still believe that random error cannot fully explain the scatter for unstable ϕ_m because we observe a clear diurnal trend in deviations of ϕ_m from theory, which suggests that ϕ_m depends on some physical quantity that varies diurnally, which is not accounted for in MOST (see Fig. 7c). For stable ϕ_h, self-correlation may be causing additional scatter, and as a result, it is possible that the χ^2 tests for stable ϕ_h are producing false negatives. Note, however, that it still may be possible to determine whether scatter in stable ϕ_h can be explained by random errors through the use of a multivariate statistical hypothesis test.

Second, note that the conclusions of Baas et al. (2006) hold regardless of the cause of the perturbations in the common quantities that appear in both the independent and the dependent variable (i.e., u_* and $\overline{w'\theta'}$). Thus, if physical processes in the ABL were to lead to different values of u_* or $\overline{w'\theta'}$ (for fixed gradients) than what would be predicted by MOST, the scatter caused by these physical processes would be easier to detect in unstable ϕ_m and stable ϕ_h, in which they would lead to more scatter, than in stable ϕ_m and unstable ϕ_h, in which much of this scatter would be suppressed by self-correlation.

7. Conclusions

Below is a summary of the main conclusions of this article.

- Flux–gradient relationships from AHATS dataset were found to have many similarities to results from the Kansas experiment (Businger et al. 1971). We obtained a value of $\kappa = 0.355$ from fits to the near-neutral velocity profiles. Our results suggest that the turbulent Prandtl number ($\text{Pr}_t = \phi_h/\phi_m$) is less than one for near-neutral conditions. Furthermore, the best-fit curves to ϕ_m and ϕ_h from our data were found to be close to the empirical fits of Businger et al. (1971) and Businger–Dyer (Dyer 1974).
- Random errors in u_*, z/L, $\partial U/\partial z$, $\partial \Theta/\partial z$, ϕ_m, and ϕ_h were estimated by propagating errors in the turbulent fluxes.
- For the unstable surface layer, random errors in u_* were found to be on the order of 10% and errors in z/L were found to be on the order of 40% or greater.
- The χ^2 tests show that random errors are not able to explain scatter in calculated values of ϕ_m or ϕ_h relative to empirical curves, which suggests that ϕ_m and ϕ_h depend on nondimensional parameters besides z/L that describe physical processes that are neglected in Monin–Obukhov similarity theory.
- It is observed that the normalized deviations of calculated values of ϕ_m from theory have diurnal variation and increase in magnitude with height; this suggests that ϕ_m depends on some quantity that

varies diurnally. Although one potential candidate for this additional dimensionless parameter is z/z_i, which would be consistent with previous studies (e.g., Khanna and Brasseur 1997; Johansson et al. 2001), we cannot conclusively determine from our present dataset what this additional dimensionless parameter is.
- In contrast to ϕ_m, the deviations of ϕ_h from theory are not found to have a significant diurnal trend and have only a weak height dependence. The deviations of ϕ_h become large near sunset, which suggests that processes related to the collapse of the convective boundary layer may lead to deviations from MOST.
- Because random errors in z/L are large for unstable stratification (e.g., on the order of 50% for $z/L = -1$), the true value of z/L is difficult to determine accurately for unstable conditions. This may be one explanation for the existence of the shaded regions in the empirical curves for the w and θ spectra proposed by Kaimal et al. (1972), where the spectra fail to collapse to a single curve for unstable conditions.

The traditional view in micrometeorology is that a large amount of scatter in measurements is unavoidable because of insufficient averaging times, which introduce random errors into the measurements. Scatter in plots of $\phi_m(z/L)$, for example, is typically attributed to random error. The AHATS experiment was conducted at a field site with predominantly level and horizontally homogeneous terrain, making it a good location to test MOST. The scatter that we observed in plots of $\phi_m(z/L)$ relative to the empirical curves was typical of many previous ASL experiments. If no error bars were plotted for z/L and ϕ_m, then one would likely conclude that the data were in good agreement with the empirical curves (see Fig. 5). However, our results indicate that the observed scatter in both ϕ_m and ϕ_h cannot be explained solely due to random error; the rest must be due to other factors, such as the dependence of ϕ_m and ϕ_h on additional nondimensional parameters that describe physical processes that are neglected in MOST. Perhaps future studies of the atmospheric surface layer should not so easily attribute scatter in measurements to random errors, but rather seek to differentiate between these errors and other physical processes that lead to departures from Monin–Obukhov similarity theory.

Acknowledgments. The authors gratefully acknowledge support from the National Science Foundation Grant AGS-0638385. The AHATS data were collected by NCAR's Integrated Surface Flux Facility.

APPENDIX

Errors in Fitted Parameters

The errors in the fitted parameters for the polynomial fit in (10) to the measured velocity and temperature profiles can be estimated by standard statistical methods (e.g., Press et al. 1986, 665–668). The uncertainties in the fitted parameters A and B are given by

$$\sigma_A^2 = \frac{\sigma^2}{\mathbf{D}} \begin{vmatrix} N & \sum_{k=1}^{N} [\ln(z_k)]^2 \\ \sum_{k=1}^{N} [\ln(z_k)]^2 & \sum_{k=1}^{N} [\ln(z_k)]^4 \end{vmatrix} \tag{A1}$$

$$\sigma_B^2 = \frac{\sigma^2}{\mathbf{D}} \begin{vmatrix} N & \sum_{k=1}^{N} [\ln(z_k)] \\ \sum_{k=1}^{N} [\ln(z_k)] & \sum_{k=1}^{N} [\ln(z_k)]^2 \end{vmatrix}, \tag{A2}$$

where $|\cdot|$ denotes the matrix determinant. Similarly, the covariance of A and B is given by

$$\mathrm{Cov}(A,B) = \frac{\sigma^2}{\mathbf{D}} \begin{vmatrix} \sum_{k=1}^{N} [\ln(z_k)] & N \\ \sum_{k=1}^{N} [\ln(z_k)]^3 & \sum_{k=1}^{N} [\ln(z_k)]^2 \end{vmatrix}, \tag{A3}$$

where

$$\mathbf{D} = \begin{vmatrix} N & \sum_{k=1}^{N} [\ln(z_k)] & \sum_{k=1}^{N} [\ln(z_k)]^2 \\ \sum_{k=1}^{N} [\ln(z_k)] & \sum_{k=1}^{N} [\ln(z_k)]^2 & \sum_{k=1}^{N} [\ln(z_k)]^3 \\ \sum_{k=1}^{N} [\ln(z_k)]^2 & \sum_{k=1}^{N} [\ln(z_k)]^3 & \sum_{k=1}^{N} [\ln(z_k)]^4 \end{vmatrix}, \tag{A4}$$

N is the number of points in the profile ($N = 6$ for the AHATS profile tower), and σ^2 is the mean square error for the fit; that is,

$$\sigma^2 = \frac{1}{N-3} \sum_{k=1}^{N} \{U(z_k) - U_0 - A\ln(z_k) - B[\ln(z_k)]^2\}^2 \tag{A5}$$

for the velocity gradient.

REFERENCES

Andreas, E. L, and B. Hicks, 2002: Comments on ''Critical test of the validity of Monin–Obukhov similarity during convective conditions.'' *J. Atmos. Sci.,* **59,** 2605–2607.

Baas, P., G. J. Steeneveld, B. J. H. van de Wiel, and A. A. M. Holtslag, 2006: Exploring self-correlation in flux–gradient relationships for stably stratified conditions. *J. Atmos. Sci.,* **63,** 3045–3054.

Baldocchi, D. D., B. B. Hincks, and T. P. Meyers, 1988: Measuring biosphere-atmosphere exchanges of biologically related gases with micrometeorological methods. *Ecology,* **69,** 1331–1340.

Banta, R., 1985: Late-morning jump in TKE in the mixed layer over a mountain basin. *J. Atmos. Sci.,* **42,** 407–412.

Beljaars, A., 1995: The parametrization of surface fluxes in large-scale models under free convection. *Quart. J. Roy. Meteor. Soc.,* **121,** 255–270.

Bernardes, M., and N. Dias, 2010: The alignment of the mean wind and stress vectors in the unstable surface layer. *Bound.-Layer Meteor.,* **134,** 41–59.

Bevington, P., and D. Robinson, 1969: *Data Reduction and Error Analysis for the Physical Sciences.* McGraw-Hill, 336 pp.

Businger, J., 1973: A note on free convection. *Bound.-Layer Meteor.,* **4,** 323–326.

——, J. Wyngaard, Y. Izumi, and E. Bradley, 1971: Flux-profile relationships in the atmospheric surface layer. *J. Atmos. Sci.,* **28,** 181–189.

Cheng, Y., M. B. Parlange, and W. Brutsaert, 2005: Pathology of Monin-Obukhov similarity in the stable boundary layer. *J. Geophys. Res.,* **110,** D06101, doi:10.1029/2004JD004923.

Cline, D., 1997: Snow surface energy exchanges and snowmelt at a continental, midlatitude Alpine site. *Water Resour. Res.,* **33,** 689–701.

Deardorff, J., 1972a: Numerical investigation of neutral and unstable planetary boundary layers. *J. Atmos. Sci.,* **29,** 91–115.

——, 1972b: Parameterization of the planetary boundary layer for use in general circulation models. *Mon. Wea. Rev.,* **100,** 93–106.

Dyer, A. J., 1974: A review of flux-profile relationships. *Bound.-Layer Meteor.,* **7,** 363–372.

Edson, J. B., and C. W. Fairall, 1998: Similarity relationships in the marine atmospheric surface layer for terms in the TKE and scalar variance budgets. *J. Atmos. Sci.,* **55,** 2311–2328.

Foken, T., 2006: 50 years of the Monin–Obukhov similarity theory. *Bound.-Layer Meteor.,* **119,** 431–447.

Fuentes, J. D., and Coauthors, 2000: Biogenic hydrocarbons in the atmospheric boundary layer: A review. *Bull. Amer. Meteor. Soc.,* **81,** 1537–1576.

Garcia, C. M., P. R. Jackson, and M. H. Garcia, 2006: Confidence intervals in the determination of turbulence parameters. *Exp. Fluids,* **40,** 514–522.

Högström, U., 1974: A field study of the turbulent fluxes of heat, water vapour and momentum at a 'typical' agricultural site. *Quart. J. Roy. Meteor. Soc.,* **100,** 624–639.

——, 1988: Non-dimensional wind and temperature profiles in the atmospheric surface layer: A re-evaluation. *Bound.-Layer Meteor.,* **42,** 55–78.

Johansson, C., A.-S. Smedman, U. Högström, J. G. Brasseur, and S. Khanna, 2001: Critical test of the validity of Monin–Obukhov similarity during convective conditions. *J. Atmos. Sci.,* **58,** 1549–1566.

——, ——, ——, and ——, 2002: Reply. *J. Atmos. Sci.,* **59,** 2608–2614.

Kaimal, J. C., J. C. Wyngaard, Y. Izumi, and R. Coté, 1972: Spectral characteristics of surface-layer turbulence. *Quart. J. Roy. Meteor. Soc.,* **98,** 563–589.

Khanna, S., and J. Brasseur, 1997: Analysis of Monin–Obukhov similarity from large-eddy simulation. *J. Fluid Mech.,* **345,** 251–286.

Klipp, C. L., and L. Mahrt, 2004: Flux-gradient relationship, self-correlation, and intermittency in the stable boundary layer. *Quart. J. Roy. Meteor. Soc.,* **130,** 2087–2103.

Lee, X., G. Benoit, and X. Hu, 2000: Total gaseous mercury concentration and flux over a coastal saltmarsh vegetation in Connecticut, USA. *Atmos. Environ.,* **34,** 4205–4213.

Lenschow, D., J. Mann, and L. Kristensen, 1994: How long is long enough when measuring fluxes and other turbulence statistics? *J. Atmos. Oceanic Technol.,* **11,** 661–673.

Li, X., N. Zimmerman, and M. Princevac, 2008: Local imbalance of turbulent kinetic energy in the surface layer. *Bound.-Layer Meteor.,* **129,** 115–136.

Louis, J., 1979: A parametric model of vertical eddy fluxes in the atmosphere. *Bound.-Layer Meteor.,* **17,** 187–202.

Lumley, J., and H. Panofsky, 1964: *The Structure of Atmospheric Turbulence.* Interscience, 239 pp.

Moeng, C.-H., 1984: A large-eddy simulation model for the study of planetary boundary-layer turbulence. *J. Atmos. Sci.,* **41,** 2052–2062.

Moncrieff, J., R. Valentini, S. Greco, S. Guenther, and P. Ciccioli, 1997: Trace gas exchange over terrestrial ecosystems: Methods and perspectives in micrometeorology. *J. Exp. Bot.,* **48,** 1133–1142.

Monin, A. S., and A. M. Obukhov, 1954: Basic laws of turbulent mixing in the atmospheric surface layer. *Tr. Geofiz. Inst., Akad Nauk SSSR,* **24,** 163–187.

Nieuwstadt, F. T. M., 1984: The turbulent structure of the stable, nocturnal boundary layer. *J. Atmos. Sci.,* **41,** 2202–2216.

Obukhov, A. M., 1946: Turbulence in an atmosphere with inhomogeneous temperature. *Tr. Inst. Teor. Geofiz., Akad Nauk SSSR,* **1,** 95–115.

Oncley, S. P., C. A. Friehe, J. C. Larue, J. A. Businger, E. C. Itsweire, and S. S. Chang, 1996: Surface-layer fluxes, profiles, and turbulence measurements over uniform terrain under near-neutral conditions. *J. Atmos. Sci.,* **53,** 1029–1044.

Panofsky, H., H. Tennekes, D. Lenschow, and J. Wyngaard, 1977: The characteristics of turbulent velocity components in the surface layer under convective conditions. *Bound.-Layer Meteor.,* **11,** 355–361.

Press, W., B. Flannery, S. Teukolsky, W. Vetterling, and B. Flannery, 1986: *Numerical Recipes in Fortran 77: The Art of Scientific Computing,* 2nd ed. Vol. 1, *Fortran Numerical Recipes,* Cambridge University Press, 933 pp.

Salesky, S. T., M. Chamecki, and N. L. Dias, 2012: Estimating the random error in eddy-covariance based fluxes and other turbulence statistics: The filtering method. *Bound.-Layer Meteor.,* **144,** 113–135, doi:10.1007/s10546-012-9710-0.

van de Wiel, B. J. H., S. Basu, A. F. Moene, H. J. J. Jonker, G.-J. Steeneveld, and A. A. M. Holtslag, 2011: Comments on ''An extremum solution of the Monin–Obukhov similarity equations.'' *J. Atmos. Sci.,* **68,** 1405–1408.

Vickers, D., and L. Mahrt, 1997: Quality control and flux sampling problems for tower and aircraft data. *J. Atmos. Oceanic Technol.,* **14,** 512–526.

Wang, J., and R. L. Bras, 2010: An extremum solution of the Monin–Obukhov similarity equations. *J. Atmos. Sci.,* **67,** 485–499.

——, and ——, 2011: Reply. *J. Atmos. Sci.,* **68,** 1409–1412.

Wyngaard, J. C., 1973: On surface layer turbulence. *Workshop on Micrometeorology,* D. A. Haugen, Ed., Amer. Meteor. Soc., 101–149.

Zilitinkevich, S., and Coauthors, 2006: The influence of large convective eddies on the surface-layer turbulence. *Quart. J. Roy. Meteor. Soc.,* **132,** 1426–1456.